ROYAL SOCIETY
OF CHEMISTRY

PAPER

Check for updates

The roto-conformational diffusion tensor as a tool to interpret molecular flexibility†

Sergio Rampino, [ID] Mirco Zerbetto [ID] * and Antonino Polimeno [ID]

Stochastic modeling approaches can be used to rationalize complex molecular dynamical behaviours in solution, helping to interpret the coupling mechanisms among internal and external degrees of freedom, providing insight into reaction mechanisms and extracting structural and dynamical data from spectroscopic observables. However, the definition of comprehensive models is usually limited by (i) the difficulty in defining – without resorting to phenomenological assumptions – a representative reduced ensemble of molecular coordinates able to capture essential dynamical properties and (ii) the complexity of numerical or approximate treatments of the resulting equations. In this paper, we address the first of these two issues. Building on a previously defined systematic approach to construct rigorous stochastic models of flexible molecules in solutions from basic principles, we define a manageable diffusive frame-work leading to a Smoluchowski equation determined by one main tensorial parameter, namely the scaled roto-conformational diffusion tensor, which accounts for the influence of both conservative and dissipative forces and describes the molecular mobility *via* a precise definition of internal–external and internal–internal couplings. We then show the usefulness of the roto-conformational scaled diffusion tensor as an efficient gauge of molecular flexibility through the analysis of a set of molecular systems of increasing complexity ranging from dimethylformamide to a protein domain.

1. Introduction

The dynamical behaviour of macromolecules in solution plays a key role in biological contexts. Dynamics is in fact responsible for generating a set of different structures of the same protein, for tuning binding properties of folded proteins (allosterism), for regulating pathways of folding and binding, and for controlling the function of disordered proteins or domains.[1,2] Accessing and understanding molecular motion is thus of primary importance in the study of these processes. In this respect, a number of techniques have been developed over the years to investigate macromolecular dynamics, both from the experimental (*e.g.*, NMR,[3] fluorescence techniques,[4] time-resolved X-ray scattering,[5] atomic force microscopy,[6] neutron spectroscopy;[7] see this last reference for a comprehensive review) and the theoretical and computational perspectives. The dynamics of macromolecules in solution can in principle be reproduced *in silico* by fully atomistic molecular dynamics (MD) simulations through popular packages

such as GROMACS, CHARMM and NAMD. However, considering a medium-size protein with a sufficient number of surrounding water molecules an order of 10^4–10^5 atoms is typically reached, and limitations due to computational cost both in terms of time and memory usage are easily met even on high-performance computing platforms. To overcome these limitations, several strategies can be pursued.

First of all, direct coarse-grained approaches have been developed over the years with the aim of reducing the number of explicitly considered degrees of freedom by collecting in some appropriate way groups of atoms into collective particles (beads) and adopting an effective force field among them, also aided by state-of-the art machine-learning techniques.[8,9] A less direct but intriguing approach is followed when distinguishing between relevant motions (or coordinates), primarily affecting the process or property under study, and non-relevant ones, which have – or are supposed to have – a negligible effect and can be treated in some suitable approximate way. This is the field of the so-called relevant dynamics: in other words, a few important details are supposed to be responsible for a phenomenon to happen, while all the others can be thought of as molecule-dependent fine tuners of the properties of the phenomenon. In these approaches, the problem is thus that of defining/finding the relevant coordinates of the system, focusing on the important, hopefully small, subset of degrees of freedom. The partition "relevant *vs.* irrelevant" can be based on purely phenomenological

Department of Chemical Sciences, University of Padova, Via Marzolo 1, I-35131, Padova, Italy. E-mail: mirco.zerbetto@unipd.it; Fax: +39 049 8275050; Tel: +39 049 8275678

† Electronic supplementary information (ESI) available: Results on the roto-conformational diffusion tensor (analogues of Fig. 2, 5 and 9) for the remaining five oligosaccharides, brief review of the Fokker–Planck equation in internal coordinates, and derivation of the Smoluchowski equation by projetion of the momenta. See DOI: https://doi.org/10.1039/d3cp01382k

14822 | *Phys. Chem. Chem. Phys.*, 2023, **25**, 14822–14835

This journal is © the Owner Societies 2023

considerations, or, at least approximately, on algorithmic procedures. In the Gaussian Network Model, for instance, the molecule is seen as an ensemble of beads interacting within a cutoff radius with a harmonic potentials of the same strength.[10,11] The diagonalization of the so-called Kirchoff matrix (worked out from the variance-covariance matrix describing the correlation between the displacements of bead pairs) leads to the definition of a set of generalized coordinates (linear combinations of Cartesian coordinates of the beads) whose relevance in terms of relaxation times is directly proportional to the amplitude of the motion given by the related eigenvalue. Similar alternative models are the anisotropic network model, based on the diagonalization of the Hessian of the potential instead of the Kirchoff matrix,[12,13] and the normal mode analysis, expressing the dynamics of a protein as a superposition of collective motions called normal modes.[14,15] Among other viable approaches, the filtering technique is based on the idea of removing high-frequency fast motions with a low pass filter applied to a Fourier transformed MD trajectory,[16,17] to focus on the structural and energetic features of low-frequency collective motions. Singular Value Decomposition is thought to be very useful for characterization of the nonlinear dynamics of multivariate systems and to the identification of the dominant modes of motion in systems whose cooperative dynamics cannot be fully explored within reasonable computation time using conventional simulation techniques.[18] Finally, the widely employed principal component analysis,[19] also known as essential dynamics, involves as some of the previously mentioned techniques the construction and diagonalization of a matrix which leads to the definition of collective generalized coordinates.

Once defined, the subset of relevant coordinates can be described using stochastic approaches, which are particularly useful when discussing molecules in solutions. The definition of a comprehensive approach to define molecularly-based Fokker–Planck (FP) models can be conducted within a general framework. In our previous work[20,21] we gave a contribution to the definition of a general procedure to derive a FP description by addressing the relaxation processes of a flexible (macro)-molecule as a non-rigid body, based on a generic set of internal and external degrees of freedom, which define a Markovian process. This was pursued by first setting up the Liouville equation of motion[22] for a generic flexible body defined as a set of material points (atoms or beads), in terms of roto-translational and natural internal coordinates. The general description of a macromolecule in solution was then carried out in terms of a collection of flexible bodies, to which a standard Nakajima-Zwanzig[23,24] projection method was applied in order to eliminate the irrelevant, *i.e.* not directly observed, degrees of freedom. A generalized master equation was obtained. Alternative modeling options, based on different choices of the internal variables, of accuracy levels of the description of solvents effects, *etc.*, were reviewed. The case of a partially rigid Brownian rotator (semi-flexible body model), *i.e.* with only internal modes described by a harmonic internal energy, was discussed.[21]

The resulting theoretical approach, while effective, is still considerably challenging from a computational point of view. To partially overcome this limitation, we propose here to simplify the general scheme[20,21] by projecting out all the conjugate momenta. Such an approximation is valid in the diffusive limit, and leads to the Smoluchowski description of the stochastic motion of the relevant coordinates only. We present in particular in this paper first, for sake of completeness, the derivation of the diffusive description from the general model, and then we concentrate on the characteristics of the main tensorial parameter defining the resulting FP equation, *i.e.* the (scaled) roto-conformational diffusive tensor, **D**, which includes, at least for semi-flexible systems not undergoing large amplitude internal motions, information on both the molecular internal energy landscape and the dispersive medium. In particular, we intend to test the usefulness of **D** as a gauge of molecular flexibility. We argue that, by analysing in different ways the tensor elements, its eigenvalues spectrum and other derived quantities, it is possible to acquire additional insight into the molecular mobility. To do so, after sketching the theoretical framework in Section 2, we analyze in Section 3 the features of the roto-conformational diffusion tensor for molecular systems of increasing complexity, ranging from the simple dimethylformamide to a protein domain, and we discuss its possible role as a signature for measuring the dynamical relevance of subsets of coordinates. Conclusions are drawn in Section 4 and some perspectives are outlined.

2. Roto-conformational diffusive equation

Following ref. 20 and 21 (neglecting translational degrees of freedom) we can identify for a generic non-rigid molecule in a homogeneous medium a set of rotational coordinates (**Ω**) defined with respect to some convenient instantaneous molecular frame and the related angular momentum (**L**) as external variables, coupled with a set of internal generic coordinates and their momenta (**q**, **p**). A detailed summary of the basic hypotheses required to derive a complete non-Hermitian FP equation for the conditional probability of the system can be found in the ESI,† for the interested reader. From eqn (S1) of the ESI,† several sources of couplings can be observed: inertial coupling between coordinates and momenta, precession terms, kinetic coupling related to the generalized intertia tensor in the kinetic energy, friction coupling, *i.e.* dissipative forces resulting from the full friction tensor including non-zero roto-conformational blocks. All these quantities are shape dependent, *i.e.* they are defined by tensors, which are functions of **q**.

This picture is somewhat simplified when a diffusive limit is considered, *i.e.* when it is assumed that momenta **L**, **p** relax much faster then positional coordinates **Ω**, **q**. This is a reasonable approximation, usually introduced when discussing molecular relaxation processes in normal fluids at room temperature. The original complete FP equation discussed in ref. 20 and 21, can be therefore simplified by the rigorous elimination (*via* projection) of the momenta, which are considered as fast relaxing modes. The resulting time evolution operator in the reduced configuration space **Ω**, **q** is Hermitian (or easily reduced to a Hermitian form),

This journal is © the Owner Societies 2023

Phys. Chem. Chem. Phys., 2023, **25**, 14822–14835 | **14823**

allowing for a considerably increased efficiency in the subsequent numerical treatment, without renouncing to the full inclusion of internal degrees of freedom, based on non-phenomenological assumptions. The procedure employed to project the momenta follows a standard Nakajima–Zwanzig[23–25] formalism, and is sketched in the ESI† for the sake of completeness. The result is the diffusive (Smoluchowski) equation for the time dependent conditional probability $\rho(\mathbf{x},t)$ with $\mathbf{x} = (\mathbf{\Omega}, \mathbf{q})$, obtained after averaging out all the momenta $\mathbf{L}$, $\mathbf{p}$

$$\frac{\partial}{\partial t}\rho(\mathbf{x}, t) = -\hat{\Gamma}_{\mathrm{D}}\rho(\mathbf{x}, t) = \nabla_{\mathbf{x}}^{\mathrm{tr}}\mathbf{D}\rho(\mathbf{x})\nabla_{\mathbf{x}}\rho(\mathbf{x})^{-1}\rho(\mathbf{x}, t) \quad (1)$$

here $\nabla_{\mathbf{x}}$ is the gradient operator in $\mathbf{x}$, $\rho(\mathbf{x})$ is the equilibrium Boltzmann distribution with respect to the internal energy $U(\mathbf{x})$, $\mathbf{D} = k_{\mathrm{B}}T\xi^{-1}$ is the roto-conformational diffusion tensor, obtained as the inverse of the roto-conformational, shape dependent, friction tensor $\xi(\mathbf{x})$. Potential $U(\mathbf{x})$ and friction tensor $\xi(\mathbf{x})$ can be obtained from molecular information (force fields or direct quantum mechanical estimates for U; hydrodynamic models or MD trajectories for ξ). Averaging out all momenta leads, not surprisingly, to the disappearance of "mechanical" coupling; internal and external degrees freedom are therefore coupled only by friction terms, at least for a system moving in isotropic environments in which the internal energy is independent from the orientation of the molecular frame in the laboratory frame. A generic correlation function for observables depending upon $\mathbf{x}$ only can then be obtained in the diffusive limit

$$G(t) = \langle f(\mathbf{x})| \exp(-\hat{\Gamma}_{\mathrm{D}}t)|g(\mathbf{x})\rho(\mathbf{x})\rangle_{\mathbf{x}} = \langle f(\mathbf{x})|\rho(\mathbf{x}, t)\rangle_{\mathbf{x}} \quad (2)$$

where the latter equivalence is valid for $\rho(\mathbf{x},0) = g(\mathbf{x})\rho(\mathbf{x})$. Following ref. 21, we shall limit our analysis here to the case of quadratic internal energy of the form

$$U = \frac{1}{2}(\mathbf{q} - \mathbf{q}_0)^{\mathrm{tr}}\mathbf{K}(\mathbf{q} - \mathbf{q}_0) \quad (3)$$

which was defined as the semi-flexible body model in ref. 20 and 21. We define the set of scaled, shifted and internal coordinates $\mathbf{z} = \mathbf{T}\mathbf{K}^{1/2}(\mathbf{q} - \mathbf{q}_0)(k_{\mathrm{B}}T)^{-1/2}$, and we use the symmetrized form of eqn (2); matrix $\mathbf{T}$ assures that the resulting block of the diffusion tensor for internal variables is diagonal. We also rotate the initial molecular frame, chosen essentially in arbitrary way, to a new frame which assures that the block of the diffusion tensor for the orientation variables is also diagonal. Summarizing, using again the collective symbols $\mathbf{\Omega}$ for the oriental coordinates (but in the new frame) and $\mathbf{x}$ for the total configuration space $\mathbf{\Omega}$, $\mathbf{z}$ we are left with the following problem

$$\frac{\partial}{\partial t}\tilde{\rho}(\mathbf{x}, t) = -\tilde{\Gamma}_{\mathrm{D}}\tilde{\rho}(\mathbf{x}, t) = \rho(\mathbf{x})^{-1/2}\nabla_{\mathbf{x}}^{\mathrm{tr}}\mathbf{D}\rho(\mathbf{x})\nabla_{\mathbf{x}}\rho(\mathbf{x})^{-1/2}\tilde{\rho}(\mathbf{x}, t) \quad (4)$$

with

$$\rho(\mathbf{x}) = \frac{1}{8\pi^2}\frac{1}{(2\pi)^{N/2}}\exp(-z^2/2), \quad (5)$$

and

$$\mathbf{D} = \begin{pmatrix} \mathbf{D}^{(\mathrm{RR})} & \mathbf{D}^{(\mathrm{RS})} \\ \mathbf{D}^{(\mathrm{RS})\mathrm{tr}} & \mathbf{D}^{(\mathrm{SS})} \end{pmatrix}. \quad (6)$$

Here $\mathbf{D}^{(\mathrm{RR})}$ is the diagonal pure rotation diffusion matrix (3×3), $\mathbf{D}^{(\mathrm{SS})}$ is the diagonal pure internal diffusion matrix ($N \times N$), $\mathbf{D}^{(\mathrm{RS})}$ is the coupling matrix ($3 \times N$), and tr stands for matrix transposition. The time evolution operator is Hermitian. The scaled roto-conformational diffusion tensor is the key tensorial parameter here: it conflates together both the influence of conservative (rising from U) and dissipative (from friction) forces, describing the molecular mobility via a precise definition of internal–external and internal–internal couplings. Correlation functions as given in eqn (2), can now be evaluated by numerically solving eqn (4), and the Hermitian structure and Gaussian dependence of $\rho(\mathbf{x})$ allow efficient treatments. In this contribution we concentrate the discussion on the rich structure of the scaled roto-conformational tensor and its possible usefulness as an indicator of molecular flexibility.

3. Results

3.1 Systems

An ensemble of eight molecular systems of increasing complexity has been analyzed (see Fig. 1). The simplest system is dimethyl-formamide (**DMF** hereinafter), with 12 atoms and 30 internal degrees of freedom. Then follows a series of six oligosaccharides constituted by 2 to 8 sugar units, number of atoms ranging from 46 to 168, and number of internal degrees of freedom ranging from 132 to 498:

- α-L-Rhap-α-(1 → 2)-α-L-Rhap-OMe (**R2R**, 2 residues)
- β-D-Glcp-(1 → 6)-α-D-[6-^{13}C]-Manp-OMe (**BGL**, 2 residues)
- β-D-Glcp-(1 → 3)[β-D-Glcp-(1 → 2)]-α-D-Manp-OMe (**GGM**, 3 residues)
- α-D-Manp-(1 → 2)-α-D-Manp-(1 → 6)-α-D-[6-^{13}C]-Manp-OMe (**TRI**, 3 residues)
- α-L-Fucp-(1 → 2)-β-D-Galp-(1 → 3)-β-D-GlcpNAc-(1 → 3)-β-D-Galp-(1 → 4)-D-Glcp (**LNF**, 5 residues)
- γ-cyclodextrin (**GCY**, 8 residues)

The last (and most complex) considered system is **GB3** protein (PDB id: 1P7F), with 56 amino acid residues, 862 atoms and 2580 internal degrees of freedom. The orientation of the molecular frame is defined by three consecutively bonded atoms as follows: the origin coincides with the position of the second atom, the first atom lies on the negative x axis, and the third atom lies in the xy plane. For **DMF** and for the oligosaccharides the first two atoms were selected as the hydrogen and the carbon, respectively, of a plausible NMR probe (either CH or CH$_2$); for **GB3** the triplet of atoms defining the orientation frame was chosen as the first three atoms (NCC) of the polymer backbone. Fig. 1 shows the molecular structures of the considered systems with the above mentioned triplets of atoms highlighted as spheres.

In the hydrodynamic model used to evaluate the friction tensor, four quantities are required, namely: the temperature,

14824 | *Phys. Chem. Chem. Phys.*, 2023, **25**, 14822–14835

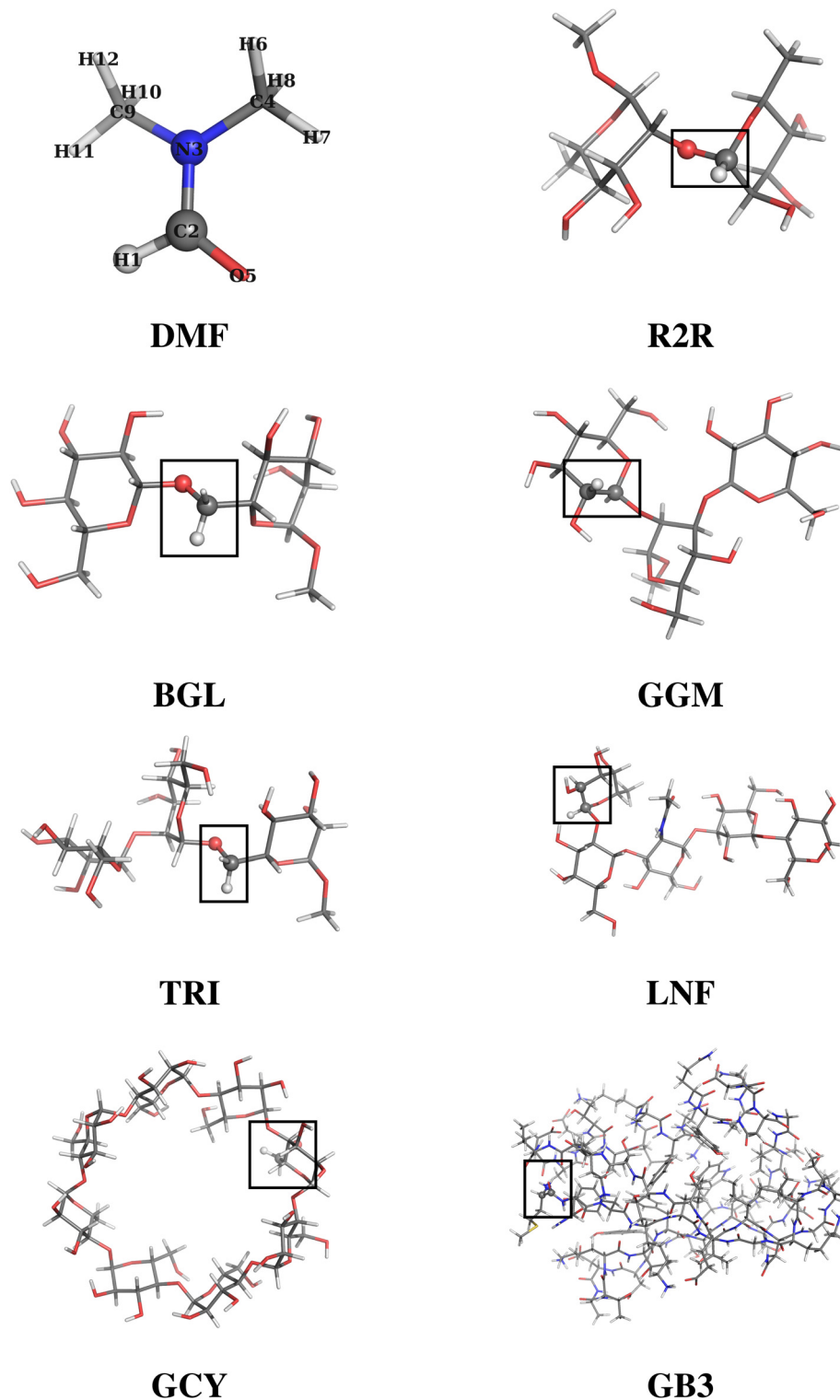This journal is © the Owner Societies 2023

Fig. 1 Three-dimensional representations of the molecular structures of the eight considered systems. The three atoms defining the orientation reference frame (see text for discussion) are highlighted as spheres.

the local viscosity, the hydrodynamic boundary conditions and the effective radius of the atoms, R_{eff}. For the set of oligosaccharides, temperature and viscosity were chosen among those for which experimental NMR data are available (see ref. 26–30), and R_{eff} was set to the optimal value providing the lowest sum

of squared percentage deviations for T_1, T_2 and NOE over the entire ensemble of experimental data available for each system, as estimated in ref. 31. For **DMF** and **GB3**, temperature and viscosity were arbitrarily chosen, and a value of R_{eff} = 2.0 Å was used. For all systems stick boundary conditions were applied.

This journal is © the Owner Societies 2023

Phys. Chem. Chem. Phys., 2023, **25**, 14822–14835 | **14825**

Table 1 Summary of the parameters of the hydrodynamic model used for the eight considered systems temperature (T), viscosity (η), and effective radius (R_{eff}). Stick boundary conditions have been assumed in all the calculations

	DMF	R2R	BGL	GGM	TRI	LNF	GCY	GB3
T/K	298.15	298.2	253.0	298.6	298.0	303.0	323.0	298.15
η/cP	2.19	2.19	2.82	1.09	3.66	1.40	2.90	0.91
R_{eff}/Å	2.0	1.6	1.8	1.8	2.2	3.2	1.8	2.0

A summary of the parameters used for all the considered systems is provided in Table 1. Calculations were performed according to the computational protocol described in the ESI.†

3.2 Rotational part of the diffusion tensor

In Table 2, the following three sets of values are reported for each systems in units of fs^{-1}:

1. elements $D_i^{(RR)} \equiv D_{ii}^{(RR)}$ of the diagonal rotational block $\mathbf{D}^{(RR)}$ of $\mathbf{D}$

Table 2 Elements of the diagonal rotational block $\mathbf{D}^{(RR)}$ of the roto-conformational diffusion tensor $\mathbf{D}$, first three of eigenvalues of the roto-conformational diffusion tensor $\mathbf{D}$, and eigenvalues of the rigid-molecule rotational diffusion tensor for the eight considered systems. Units are fs^{-1}

	$i = 1$	$i = 2$	$i = 3$
DMF			
$D_i^{(RR)}$	6.69×10^{-6}	1.26×10^{-5}	2.22×10^{-5}
$(egv[\mathbf{D}])_i$	1.82×10^{-6}	2.04×10^{-6}	2.14×10^{-6}
Rigid mol.	1.83×10^{-6}	2.15×10^{-6}	2.21×10^{-6}
R2R			
$D_i^{(RR)}$	1.05×10^{-5}	1.98×10^{-5}	3.24×10^{-5}
$(egv[\mathbf{D}])_i$	5.19×10^{-7}	5.75×10^{-7}	7.53×10^{-7}
Rigid mol.	5.24×10^{-7}	5.78×10^{-7}	7.66×10^{-7}
BGL			
$D_i^{(RR)}$	5.46×10^{-7}	1.03×10^{-6}	1.66×10^{-6}
$(egv[\mathbf{D}])_i$	2.56×10^{-8}	2.81×10^{-8}	4.47×10^{-8}
Rigid mol.	2.58×10^{-8}	2.83×10^{-8}	4.54×10^{-8}
GGM			
$D_i^{(RR)}$	1.60×10^{-5}	3.14×10^{-5}	5.00×10^{-5}
$(egv[\mathbf{D}])_i$	5.65×10^{-7}	6.57×10^{-7}	7.95×10^{-7}
Rigid mol.	5.70×10^{-7}	6.65×10^{-7}	8.08×10^{-7}
TRI			
$D_i^{(RR)}$	3.33×10^{-6}	6.24×10^{-6}	9.91×10^{-6}
$(egv[\mathbf{D}])_i$	1.35×10^{-7}	1.42×10^{-7}	2.39×10^{-7}
Rigid mol.	1.36×10^{-7}	1.43×10^{-7}	2.43×10^{-7}
LNF			
$D_i^{(RR)}$	4.04×10^{-6}	7.87×10^{-6}	1.22×10^{-5}
$(egv[\mathbf{D}])_i$	1.40×10^{-7}	1.47×10^{-7}	2.23×10^{-7}
Rigid mol.	1.42×10^{-7}	1.49×10^{-7}	2.27×10^{-7}
GCY			
$D_i^{(RR)}$	6.79×10^{-6}	1.28×10^{-5}	2.03×10^{-5}
$(egv[\mathbf{D}])_i$	9.54×10^{-8}	1.12×10^{-7}	1.22×10^{-7}
Rigid mol.	9.63×10^{-8}	1.13×10^{-7}	1.23×10^{-7}
GB3			
$D_i^{(RR)}$	1.37×10^{-5}	2.26×10^{-5}	4.01×10^{-5}
$(egv[\mathbf{D}])_i$	5.35×10^{-8}	5.79×10^{-8}	7.62×10^{-8}
Rigid mol.	5.41×10^{-8}	5.84×10^{-8}	7.67×10^{-8}

2. first three eigenvalues of the set of eigenvalues obtained by full diagonalization of $\mathbf{D}$ and sorted in ascending order.

3. eigenvalues of the rotational diffusion tensor for the rigid molecule obtained with the DiTe2 software package,[32] using the same hydrodynamic model and the same conditions described above.

A strikingly good agreement is found between the eigenvalues of the rotational diffusion tensor of the rigid molecule (set 3) and the lowest three eigenvalues of the (fully diagonalized) $\mathbf{D}$ matrix (set 2). Therefore, upon coordinate transformation the diagonalization of $\mathbf{D}$ seems to lead to a separation of motions, with the three separated eigenvalues being close to the rotational diffusion of the molecule as if it was rigid. The two sets of eigenvalues show an overall decreasing trend with increasing systems size and complexity. In contrast, the three elements of the diagonal rotational block of $\mathbf{D}^{(RR)}$ (set 1) do not exhibit a clear trend with increasing system size, and except for the first (and smallest) system their values are one or two orders of magnitude smaller than the respective values from the other two sets. This is in line with the fact that the elements of $D_i^{(RR)}$ relate to the rotation of a small subsystem made of the triplet of atoms used to define the molecular frame.

3.3 Analysis of the roto-conformational diffusion tensor

Interesting information can be gained through the analysis of the remaining blocks of the roto-conformational diffusion tensor $\mathbf{D}$. In fact, the diagonalization of the conformational block of the diffusion tensor leads to the definition of a set of 'normal modes', each defined by an eigenvector (a column of the $\mathbf{T}$ matrix) and associated to a given eigenvalue $D_i^{(SS)} \equiv D_{ii}^{(SS)}$ which has units of a frequency. These normal modes are linear combinations of the original set of internal coordinates $\mathbf{q}$ with coefficients being the elements of the respective eigenvector. Their character, in terms of their motion, can be thus inferred by the analysis of these coefficients. In particular, the contribution to a given j-th normal mode coming from the motion associated with a given internal coordinate q_i can be estimated as the square of the matrix element T_{ij}, with the squares of the element of each j-th column of $\mathbf{T}$ summing up to one.

On the other hand, the analysis of the elements of the roto-conformational block $\mathbf{D}^{(SR)}$ provides information on the coupling between the internal degrees of freedom and the external rotation.

'Normal modes' and coupling with external motion in DMF. Focusing on the simplest considered system, **DMF**, Fig. 2 shows the values of the diagonal conformational block $D^{(SS)}$ (panel c), the values of the elements of the roto-conformational block $D_{ij}^{(SR)}$ divided by $|D_i^{(SS)} - D_j^{(RR)}|$, so as to provide an indication of the importance of the coupling (panel d), and the square of the elements of the $\mathbf{T}$ matrix (panel b). The molecular structure is also shown for reference (panel a). The rows of the $\mathbf{T}$ matrix (panel b) have been reordered so as to group together first the stretchings, then the bendings, and finally the torsions. Each row is labeled with a string indicating the kind of motion ('S' for stretching, 'B' for bending, 'T' for torsion) and the IDs of the atoms associated with that motion, listed in the same
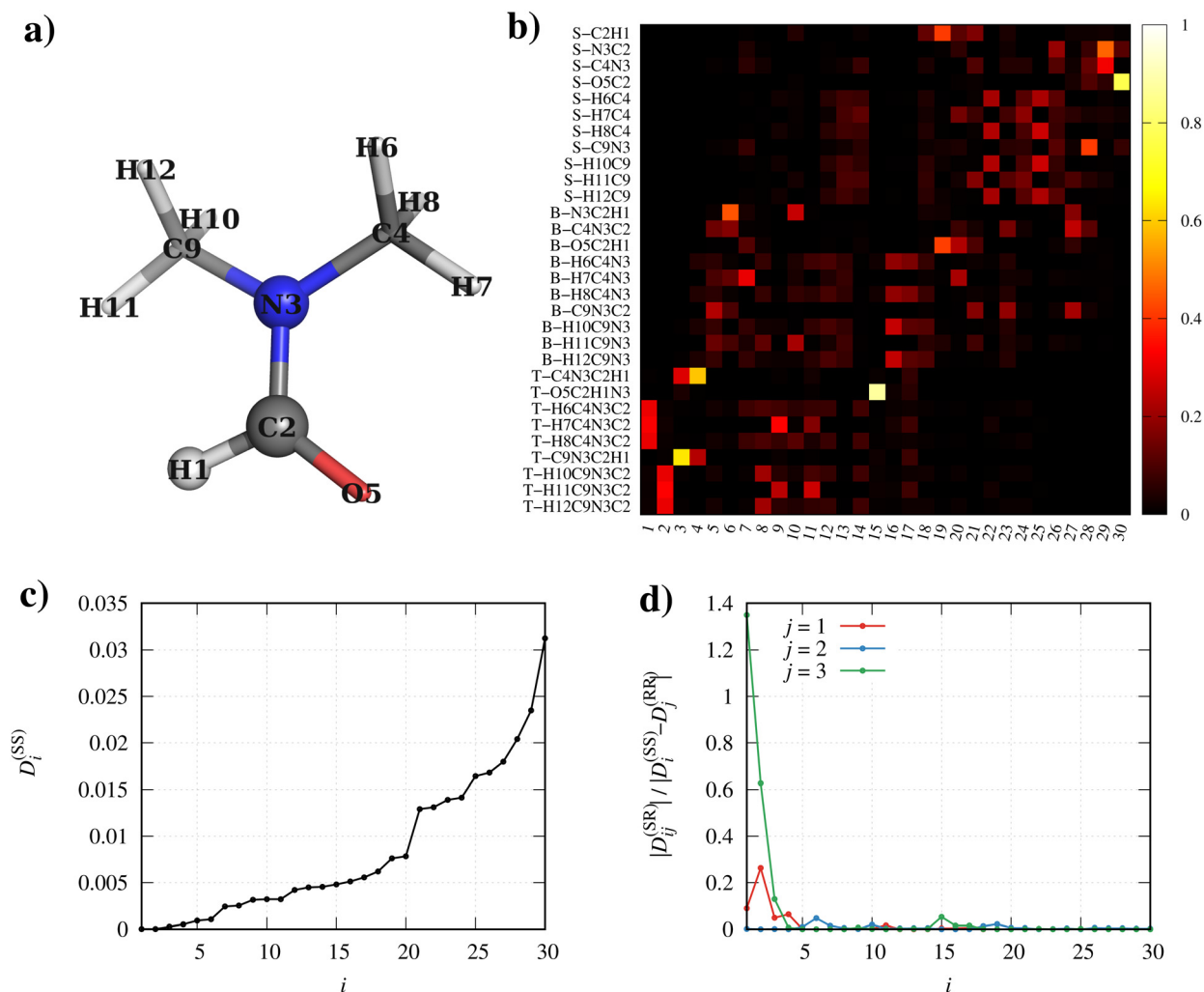
a)

b)

c)

d)

Fig. 2 (a) Molecular structure of **DMF**. (b) Color plot of the elements $T_{ij}{}^2$ of the matrix diagonalizing the internal block (SS) of the diffusion matrix. Each row is labeled with a string indicating the kind of motion ('S' for stretching, 'B' for bending, 'T' for torsion) and the IDs (see panel a) of the atoms associated with that motion, listed in the same order as they appear in the Z matrix. (c) Elements $D_i^{(SS)}$ (in fs^{-1}), *i.e.* eigenvalues of the internal block (SS) of the diffusion matrix. (d) Extent of the coupling between the internal motions (each described by the i the normal mode) and the overall rotation.

order as they appear in the Z matrix. These IDs are the same that appear as atom labels in panel a. We start our analysis from the elements of the diagonal block $\mathbf{D}^{(SS)}$ (panel c). These show a monotonic trend with a few more or less evident discontinuities which suggest the breaking of the overall set of values in three frequency ranges: $i \in [1,6]$, $[7,20]$ and $[21,30]$. Looking now at the color plot of the squared elements of the **T** matrix (panel b), one sees that high values of $D_i^{(SS)}$ are associated mainly with stretching motions, intermediate values of $D_i^{(SS)}$ are associated mainly with bending motions, and low values of $D_i^{(SS)}$ are associated mainly with torsions.

The roto-conformational coupling (panel d) is strong (high values of $|D_{ij}^{(SR)}|/|D_i^{(SS)} - D_j^{(RR)}|$) for only a few normal modes with the lowest frequencies (thus mainly represented by torsion motions). In particular, the first two normal modes exhibit by far the highest coupling with external rotation, while the remaining modes turn out to be negligibly coupled to it. The analysis of the squared elements of the first two columns of

the **T** matrix (panel b) reveals that the internal motions mostly coupled with the external rotation are the C2–N3–C–H torsions (see panel a for atom numbering), with the last two atoms being one of the three CH pairs of each methyl group.

A measure of the 'coldness'/'hotness' of the atoms (*i.e.* the involvement of atoms in motions associated with lower or higher frequencies), can be computed as follows:

$$\text{'hotness' of atom } a = \frac{1}{n^{(a)}} \sum_j \sum_i D_j^{(SS)} |T_{ij}^{(a)}|^2 \qquad (7)$$

where the $T_{ij}^{(a)}$'s are the elements of the **T** matrix relating to internal coordinates (of the **q** set) featuring atom a, and $n^{(a)}$ is the number of internal coordinates (of the **q** set) featuring that atom. In other words this yields for each atom an average frequency which is worked out from the frequencies associated with the motions involving that atom, weighed by the squared elements of the **T** matrix. These atomic average frequencies can
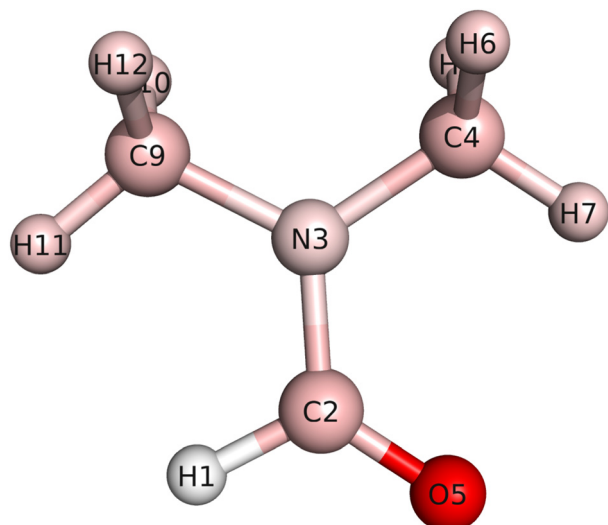
This journal is © the Owner Societies 2023

Phys. Chem. Chem. Phys., 2023, **25**, 14822–14835 | **14827**

Fig. 3   Atomic average frequencies in **DMF** computed as per eqn (7) (see text for discussion).

('coldest' atom, *i.e.* lowest frequency) to red ('hottest' atom, *i.e.* highest frequency). The figure shows that, upon adoption of the internal coordinates listed in the row labels of panel a, the hottest and coldest atoms turn out to be the O5 oxygen and the H1 hydrogen, respectively. This derives from the fact that O5 is mainly involved in the O5–C2 stretching, which strongly participates to normal mode $j = 30$ featuring the highest frequency eigenvalue, and in only one additional bending and one additional torsion. On the other hand, H1 is involved in one stretching, two bendings, and three torsions and thus participates mainly in lower-frequency modes. The average frequencies of the remaining atoms lie in an intermediate range due to the fact that their contribution in low- and high-frequency modes is more even than the two extremes O5 and H1.

One may further push the analysis to the contribution of each atom in a given type of motion (stretchings, bendings, torsions) for a given frequency range. To this purpose the following expression can be used:

be plotted for visualization purposes using a color scale for each atom as in Fig. 3, where the color ranges from white

$$\text{contribution of atom } a = \frac{1}{n^{(a)}} \sum_{j\in[\text{freq. range}]} \sum_{i\in[\text{mode type}]} |T_{ij}^{(a)}|^2 \quad (8)$$

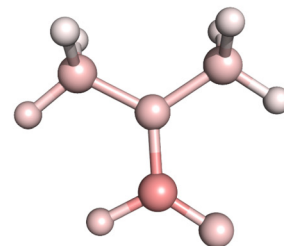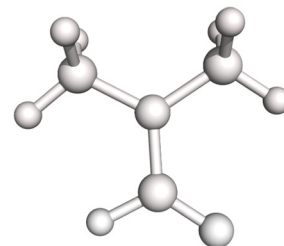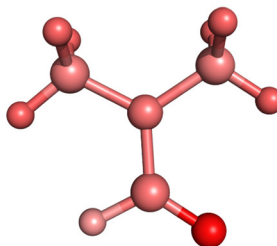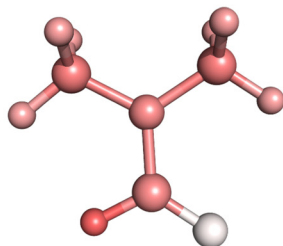| freq. range:	$D_1^{(SS)}$-$D_6^{(SS)}$	$D_7^{(SS)}$-$D_{20}^{(SS)}$	$D_{21}^{(SS)}$-$D_{30}^{(SS)}$
stretchings			
bendings			
torsions			
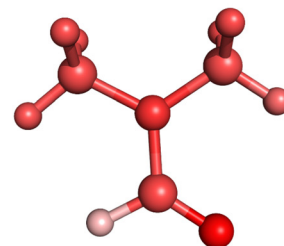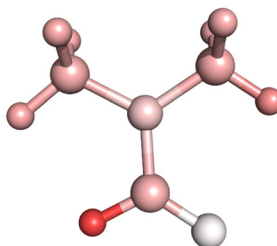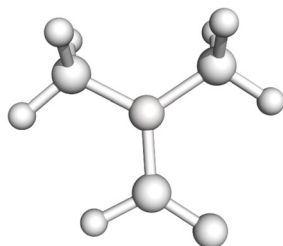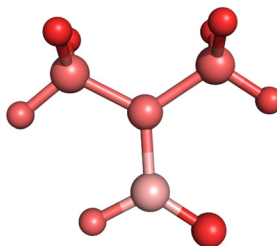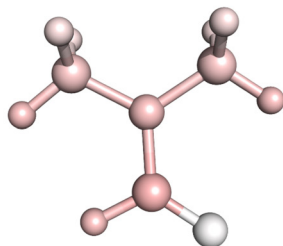
Fig. 4   Contribution of the atoms of **DMF** to stretchings, bendings and torsions in three different frequency ranges (see text for discussion).
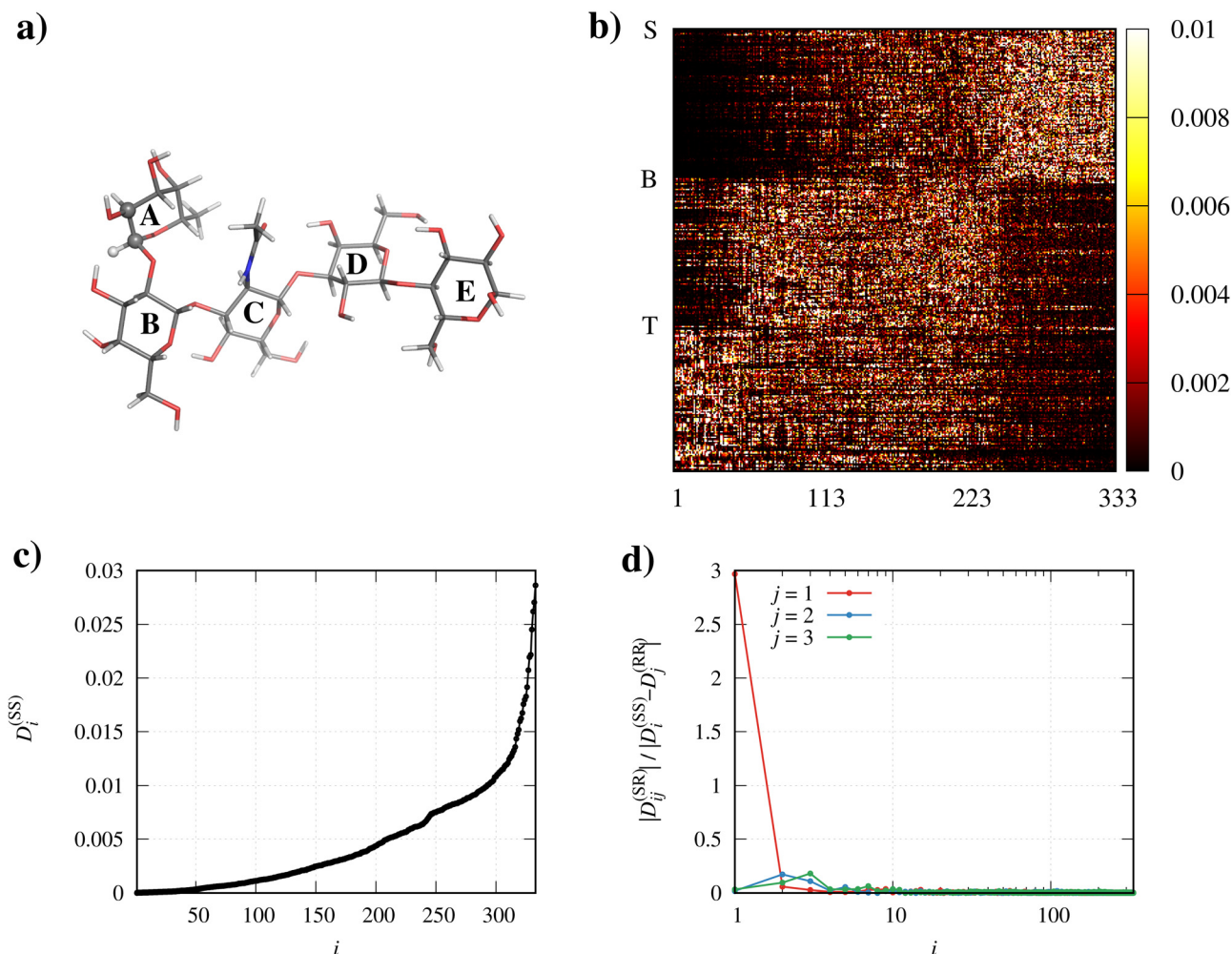
Fig. 5 (a) Molecular structure of **LNF**, with sugar units labeled with letters from A to E. (b) Color plot of the elements T_{ij}^2 of the matrix diagonalizing the internal block (SS) of the diffusion matrix. The initial row of the stretchings block (rows 1–112), of the bendings block (rows 113–222), and of the torsions block (rows 223–333) is labeled with 'S', 'B', and 'T', respectively. (c) Elements $D_i^{(SS)}$ (in fs^{-1}), i.e. eigenvalues of the internal block (SS) of the diffusion matrix. (d) Extent of the coupling between the internal motions (each described by the i the normal mode) and the overall rotation (note that the abscissa is in logarithmic scale).

where $n^{(a)}$ is the number of internal coordinates (of the **q** set) of the chosen mode type featuring that atom. In eqn (8), j spans the columns of **T** associated with eigenvalues in a given frequency range, and i spans the rows of **T** associated with a given mode type. Fig. 4 summarizes the results of such analysis for **DMF**. In particular, the three above-highlighted frequency ranges (identified by the respective eigenvalue indices) [1,6], [7,20] and [21,30] and relating to different kind of motions can
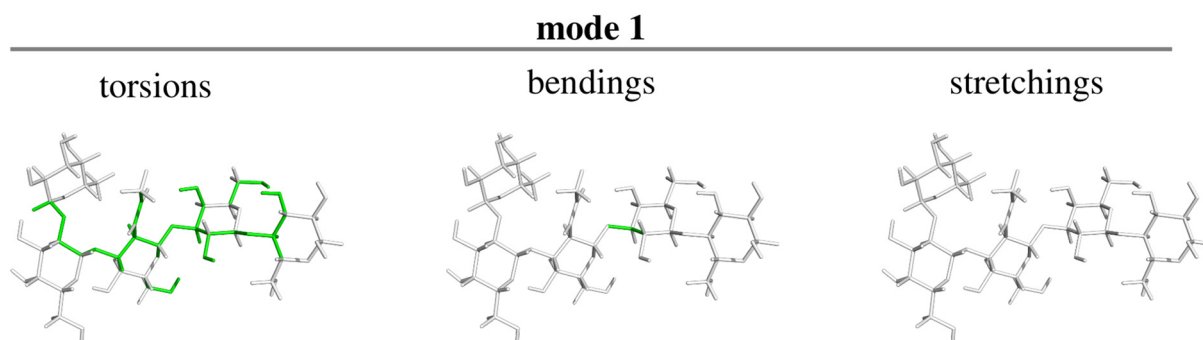
mode 1

Fig. 6 Character of the lowest frequency (and highest coupling with external motion) normal mode in terms of the constituting torsions, bendings and stretchings (see text for discussion) for **LNF**.
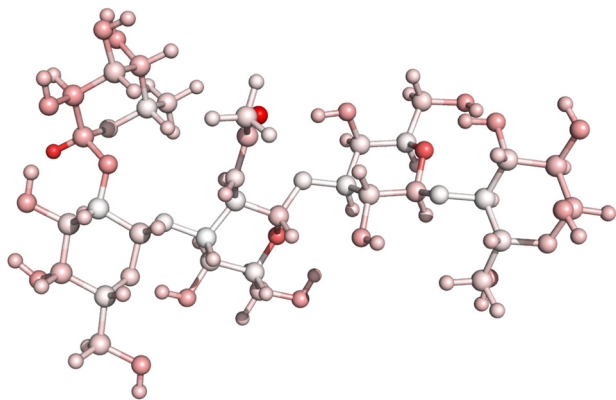
This journal is © the Owner Societies 2023

Phys. Chem. Chem. Phys., 2023, **25**, 14822–14835 | **14829**

Fig. 7 Atomic average frequencies in **LNF** computed as per eqn (7) (see text for discussion).

be conveniently adopted for this system. This results in a 3 × 3 matrix of color plots (Fig. 4), illustrating the contribution of each atom in motions of a given type for a selected frequency range. In these plots, the color scale ranges from zero (white) to one (red). As evident from Fig. 4, stretchings are the predominant kind of motions in the high frequency range, bendings are more involved in the medium frequency range (where also the C2–H1 stretching falls), and torsions are relevant in the medium and low frequency ranges. This is perfectly in line with the already discussed analysis of the elements of the **T** matrix (panel b of Fig. 2). In fact, eqn (8) converts the coordinate-related information encoded in the **T** matrix to an atom-related information, thus establishing a direct analogy between the color plot of the **T** matrix and the matrix of plots reported in Fig. 4.

'Normal modes' and coupling with external motion in pentasaccharide LNF. The features of the roto-conformational tensor for pentasaccharide **LNF** (113 atoms, 333 internal degrees of freedom) are illustrated in Fig. 5. The color plot of the squared elements of the **T** matrix in panel b shows that, analogously to the results for system **DMF**, high-frequency normal modes (approximately those in the index range [241, 333]) involve mainly stretchings while bendings and torsions contribute mainly to normal modes in the medium-low range, with torsion predominating in the bottom end (index range [1,50]). The eigenvalues $D_i^{(SS)}$ (panel c) show a smoother trend than those of the smaller system **DMF**, with a step-wise behaviour only in the region around $i = 240$, when stretching motions start to predominate.

Panel d shows that there is only one normal mode, precisely the lowest-frequency one, which is tightly coupled to the overall rotation of the molecule. The nature of this mode can be appreciated by inspection of Fig. 6, where the atom connections involved in the torsions (left panel), bendings (center panel) and stretchings (right panel) contributing to the mode with value T_{ij}^2 above a given threshold are highlighted in green. The threshold is here set to $1/N$ (with N, as already mentioned, being the number of internal degrees of freedom), *i.e.* exactly equal to the average value of all contributions to that mode by the original internal coordinates **q**. In other words, in the panels of Fig. 6, only the connections between atoms involved in motions contributing above average to the mode are highlighted.
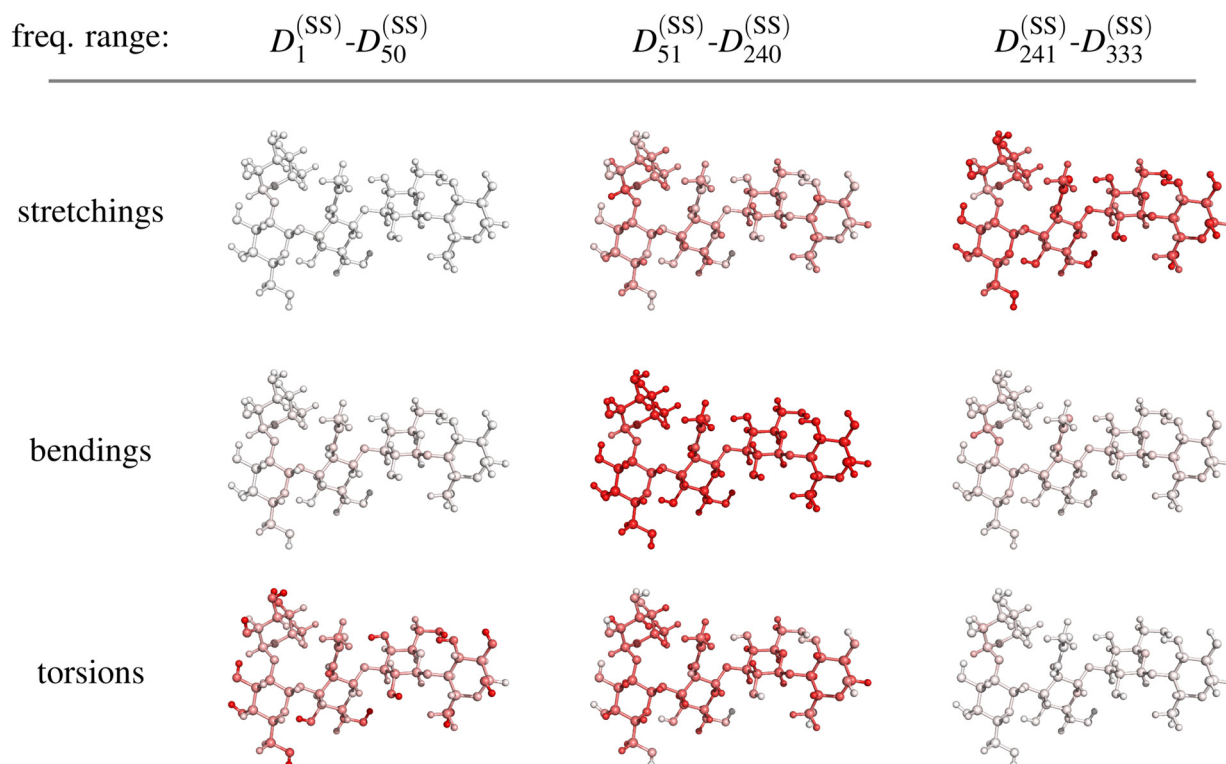
| freq. range: | $D_1^{(SS)}$-$D_{50}^{(SS)}$ | $D_{51}^{(SS)}$-$D_{240}^{(SS)}$ | $D_{241}^{(SS)}$-$D_{333}^{(SS)}$ |

Fig. 8 Contribution of the atoms of **LNF** to stretchings, bendings and torsions in three different frequency ranges (see text for discussion).

14830 | *Phys. Chem. Chem. Phys.*, 2023, **25**, 14822–14835
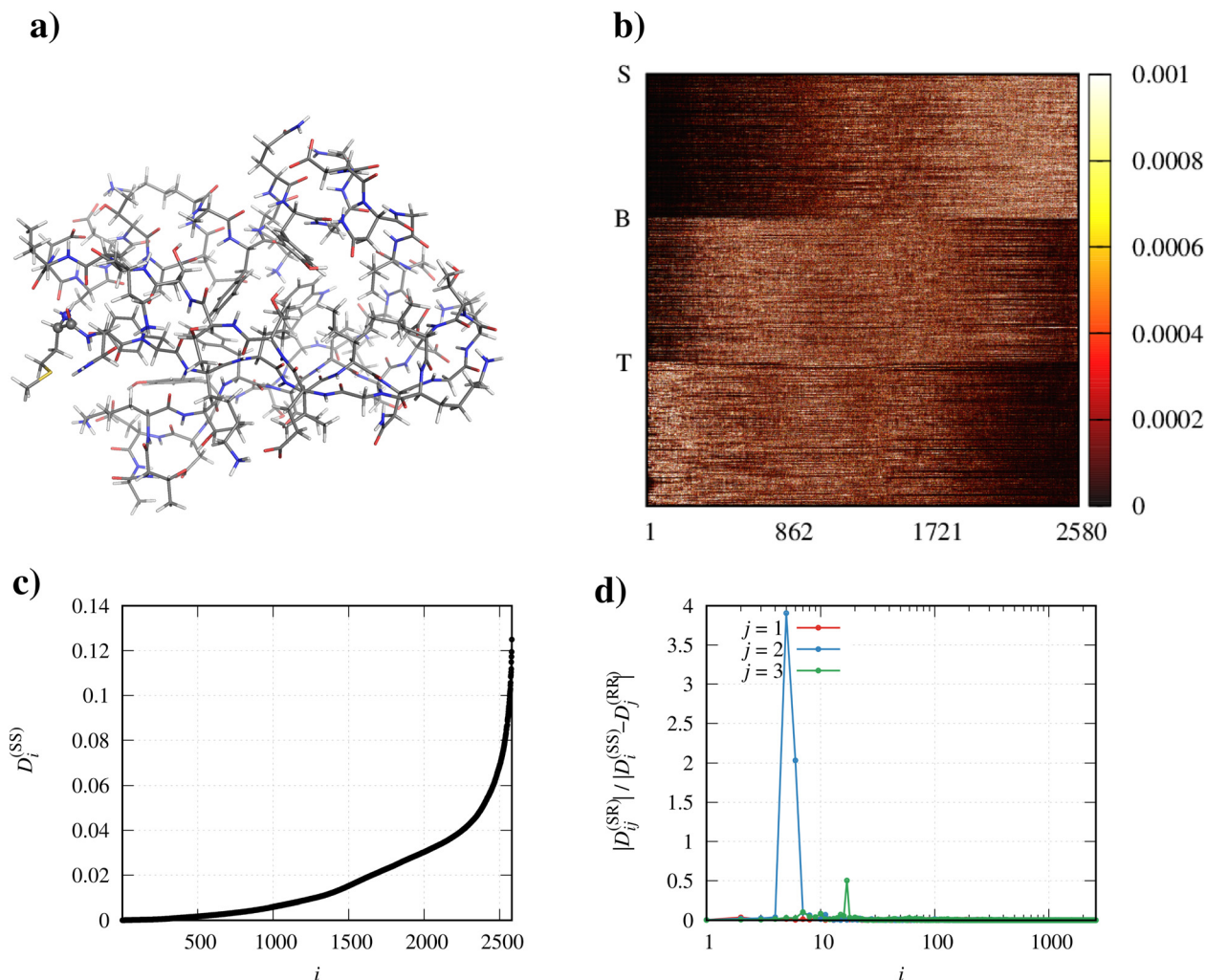
This journal is © the Owner Societies 2023

Fig. 9 (a) Molecular structure of **GB3**. (b) Color plot of the elements T_{ij}^2 of the matrix diagonalizing the internal block (SS) of the diffusion matrix. The initial row of the stretchings block (rows 1–861), of the bendings block (rows 862–1720), and of the torsions block (rows 1721–2580) is labeled with 'S', 'B', and 'T', respectively. (c) Elements $D_i^{(SS)}$ (in fs^{-1}), *i.e.* eigenvalues of the internal block (SS) of the diffusion matrix. (d) Extent of the coupling between the internal motions (each described by the i the normal mode) and the overall rotation (note that the abscissa is in logarithmic scale).
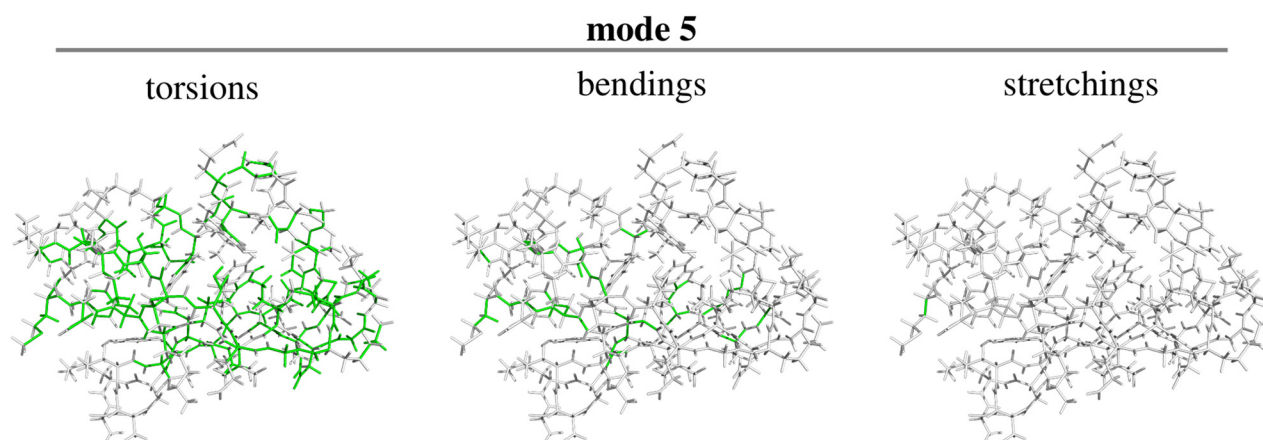

Fig. 10 Character of the fifth normal mode in terms of the constituting torsions, bendings and stretchings for **GB3** (see text for discussion).

This journal is © the Owner Societies 2023

Phys. Chem. Chem. Phys., 2023, **25**, 14822–14835 | **14831**

mode 6

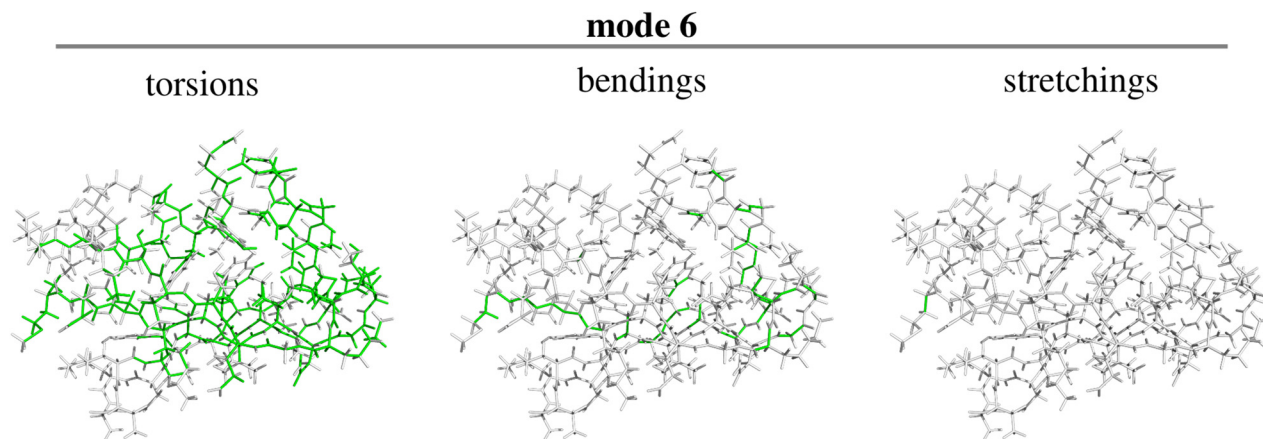| torsions	bendings	stretchings

Fig. 11 Character of the sixth normal mode in terms of the constituting torsions, bendings and stretchings for **GB3** (see text for discussion).
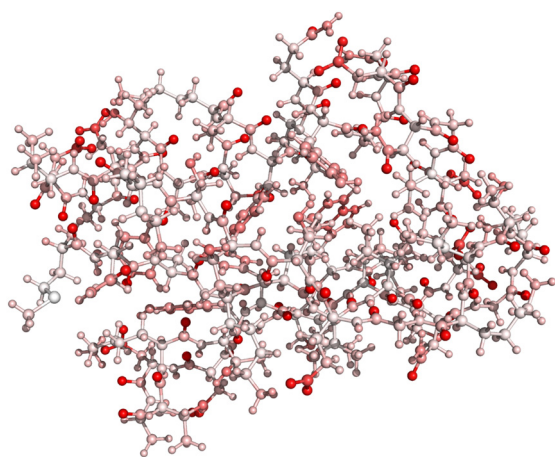

Fig. 12 Atomic average frequencies in **GB3** computed as per eqn (7) (see text for discussion).

The figure thus reveals that the only normal mode significantly coupled to the external rotation results mainly from torsions involving the atoms of the polymer backbone, plus one coordinate relating to the bending motion of three of the sugar rings with respect to the remaining two. For **LNF** we also analyzed how both the parameters relating to physical conditions and the choice of the triplet of atoms defining the orientation frame affect the above discussed results. Results are fully reported and discussed in the ESI.†

Focusing now on the atom 'hotness', Fig. 7 shows the atomic average frequencies of the atoms using the same color scale as in Fig. 3, ranging from white (coldest atom) to red (hottest atom). In this case, the hottest atom is the only terminal oxygen atom, which is bound to a single carbon atom and is thus mainly involved in the stretching of this bond. On the other hand, the coldest atoms are the carbon and oxygen atoms constituting the oligomer backbone linking the sugar rings, which are mainly involved in slow torsion motions.

Also in this case, the matrix of the color plots (Fig. 8) illustrating the contribution of the atoms in different kind of

motions for the three above envisaged frequency ranges (identified by index ranges [1,50], [51,240], and [241,333]) reflects the features of the color plot of the **T** matrix reported in panel b of Fig. 5.

'Normal modes' and coupling with external motion in protein GB3. We finally consider the case of the more complex system **GB3** (862 atoms, 2580 internal degrees of freedom). Fig. 9 summarizes the features of the roto-conformational diffusion tensor for this system. In particular, panel b shows that also for this systems, stretching motions mostly participate in the normal modes with highest frequencies (index range approximately [1801,2580]), while bendings and torsions mainly contribute to normal modes in the medium-low range, with torsions predominating in the bottom end (index range approximately [1,280]). Due to the bigger size of the molecule, the eigenvalues $D_i^{(SS)}$ (panel c) show now a smooth trend, with no apparent discontinuities. Finally, panel d reveals that only two normal modes (the fifth and the sixth in ascending order of related eigenvalue) are significantly coupled to external rotation. The nature of these two modes can be visualized through Fig. 10 and 11, where, as in Fig. 6 the atom connections involved in torsions, bendings and stretchings contributing above average to the mode are highlighted in green.

The two figures show that the modes mainly results from torsions and bendings involving the atoms of the polymer backbone, plus a stretching of the bond linking the S-methyl thioether side chain of the first (methionine) residue to the protein backbone.

The atomic average frequencies for **GB3** can be visualized in Fig. 12, where the same color scale is used as in the previously discussed Fig. 3 and 7, i.e. ranging from white (coldest atom) to red (hottest atom). In line with the results on the smaller polymer **LNF**, the hottest atoms are here the 'external' terminal oxygens, while the colder atoms are the more 'internal' carbon and nitrogen atoms constituting the polymer backbone. For this last system too, the matrix of the color plots (Fig. 13) illustrating the contribution of the atoms in different kinds of motions for the three above envisaged frequency ranges (identified by index ranges [1,280], [281,1800], and [1801,2580])
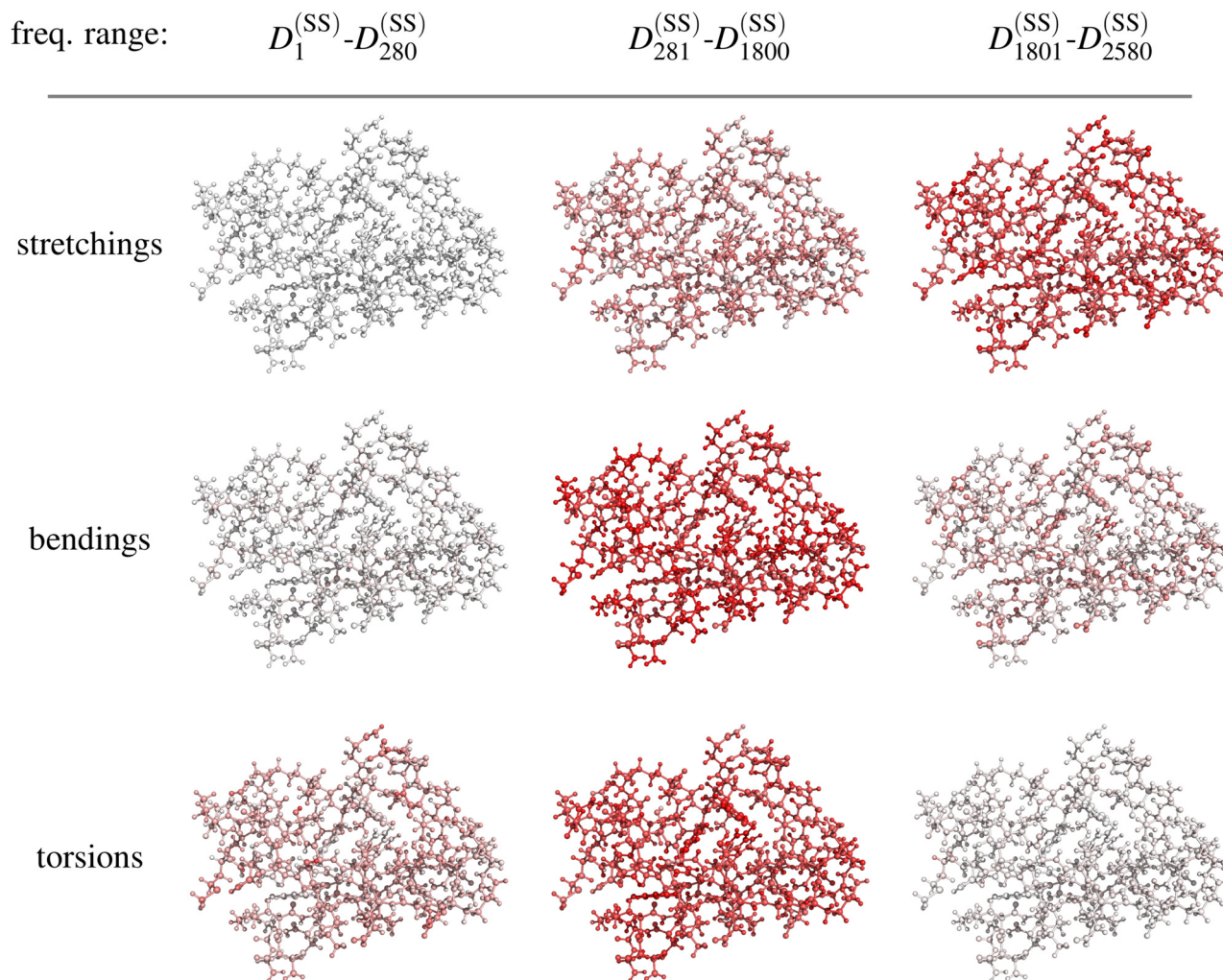
14832 | *Phys. Chem. Chem. Phys.*, 2023, **25**, 14822–14835

This journal is © the Owner Societies 2023

freq. range: $D_1^{(SS)}$-$D_{280}^{(SS)}$ $D_{281}^{(SS)}$-$D_{1800}^{(SS)}$ $D_{1801}^{(SS)}$-$D_{2580}^{(SS)}$

stretchings

bendings

torsions

Fig. 13 Contribution of the atoms of **GB3** to stretchings, bendings and torsions in three different frequency ranges (see text for discussion).

reflects the features of the color plot of the **T** matrix reported in panel b of Fig. 9.

4. Conclusions

Based on the previously defined systematic approach to build rigorous stochastic models of flexible molecules in solution from first principles,[20,21] we have considered in this paper the diffusive limit obtained upon assumption that momenta relax much faster then positional coordinates. For systems moving in isotropic environments in which the internal energy is independent from the orientation of the molecular frame in the laboratory frame, averaging out all momenta leads, not surprisingly, to a framework in which mechanical coupling disappears, and internal and external degrees freedom are coupled only by friction terms. The resulting FP equation is thus determined by one main tensorial parameter, namely the scaled roto-conformational diffusion tensor, which accounts for the influence of both conservative and dissipative forces and describes the molecular mobility *via* a precise definition of internal–external and internal–internal couplings.

Focusing on a set of molecular systems of increasing complexity ranging from dimethylformamide, to several oligosaccharides and a protein domain, we showed how the rich and informative structure of the scaled roto-conformational diffusion tensor can be analyzed to extract quantitative information on the molecular mobility. In particular, the analysis of the eigenvectors and eigenvalues of the matrix diagonalizing the conformational block of the diffusion tensor provides a quantitative picture of the time scales of the different molecular motions, putting on quantitative grounds, for instance, the time-scale separation between stretching, bending, and torsion motions. Moreover, a suitable combination of the elements of the eigenvector matrix leads to an informative definition of the 'coldness'/'hotness' of the atoms which can be used to quantitatively assess the involvement or contribution of a given atom in specific internal modes. Thus for instance, the intuitive consideration that the coldest atoms of the considered five-units oligosaccharide and protein domain are those constituting the polymer backbone, mainly involved in slow torsion motions, while the hottest atoms are the terminal oxygen atoms mainly involved in stretching motions, could be put on a

This journal is © the Owner Societies 2023

Phys. Chem. Chem. Phys., 2023, **25**, 14822–14835 | **14833**

thorough quantitative ground. Finally, the analysis of the non diagonal block of the scaled roto-conformational diffusion tensor leads to the precise determination of the few internal modes strongly coupled with the overall external rotation. The scaled roto-conformational diffusion tensor can thus be conveniently used as a gauge of molecular flexibility, also with the aim of determining a cut-off in the degrees of freedom to be included in the full solution of the related FP equation. Work is ongoing in our group on the numerical resolution of this equation with a focus on the computation of observables that can be assessed through various spectroscopic techniques including NMR and neutron spectroscopy, which simultaneously accesses spatial and time correlations (as opposed to the angular correlations probed by NMR).

The analysis of molecular flexibility presented in this work can be used as an alternative approach to the selection of essential dynamics in macromolecules, including in the analysis the flexibility in terms of characteristic time scales, instead of just energy arguments. The idea is to be able to extract such an essential dynamics (relevant coordinates) by analyzing short (with respect to the time scales required to interpret slow dynamics) MD trajectories. Machine learning techniques[33,34] are expected to be efficiently employed to pursue the best essential dynamics selection with respect to the physical observable that is being interpreted (e.g., NMR relaxation).

Author contributions

Sergio Rampino: formal analysis, investigation, conceptualization, software, validation, visualization, writing (original draft). Mirco Zerbetto: software, validation, conceptualization, resources, writing (review & editing). Antonino Polimeno: conceptualization, methodology, supervision, resources, project administration, writing (review & editing).

Conflicts of interest

There are no conflicts to declare.

Acknowledgements

Notes and references

1 T. Mittag, L. E. Kay and J. D. Forman-Kay, J. Mol. Recognit., 2009, 23, 105–116.

2 V. N. Uversky, J. R. Gillespie and A. L. Fink, Proteins, 2000, 41, 415–427.

3 D. Korzhnev, M. Billeter, A. Arseniev and V. Orekhov, Prog. Nucl. Magn. Reson. Spectrosc., 2001, 38, 197–266.

4 J. Lippincott-Schwartz, E. Snapp and A. Kenworthy, Nat. Rev. Mol. Cell Biol., 2001, 2, 444–456.

5 H. Ihee, M. Wulff, J. Kim and S. Ichi Adachi, Int. Rev. Phys. Chem., 2010, 29, 453–520.

6 T. Ando, N. Kodera, E. Takai, D. Maruyama, K. Saito and A. Toda, Proc. Natl. Acad. Sci. U. S. A., 2001, 98, 12468–12472.

7 M. Grimaldo, F. Roosen-Runge, F. Zhang, F. Schreiber and T. Seydel, Q. Rev. Biophys., 2019, 52, e7.

8 J. Wang, S. Olsson, C. Wehmeyer, A. Pérez, N. E. Charron, G. de Fabritiis, F. Noé and C. Clementi, ACS Cent. Sci., 2019, 5, 755–767.

9 P. Gkeka, G. Stoltz, A. Barati Farimani, Z. Belkacemi, M. Ceriotti, J. D. Chodera, A. R. Dinner, A. L. Ferguson, J.-B. Maillet, H. Minoux, C. Peter, F. Pietrucci, A. Silveira, A. Tkatchenko, Z. Trstanova, R. Wiewiora and T. Lelièvre, J. Chem. Theory Comput., 2020, 16, 4757–4775.

10 M. M. Triton, Phys. Rev. Lett., 1996, 77, 1905–1908.

11 D. Ben-Avraham, Phys. Rev. B: Condens. Matter Mater. Phys., 1993, 47, 14559–14560.

12 A. R. Atilgan, S. R. Durell, R. L. Jernigan, M. C. Demirel, O. Keskin and I. Bahar, Biophys. J., 2001, 80, 505–515.

13 E. Eyal, L.-W. Yang and I. Bahar, Bioinformatics, 2006, 22, 2619–2627.

14 N. Go, T. Noguti and T. Nishikawa, Proc. Natl. Acad. Sci. U. S. A., 1983, 80, 3696–3700.

15 B. Brooks and M. Karplus, Proc. Natl. Acad. Sci. U. S. A., 1983, 80, 6571–6575.

16 P. Dauber-Osguthorpe and D. J. Osguthorpe, J. Am. Chem. Soc., 1989, 112, 7921–7935.

17 P. Dauber-Osguthorpe and D. J. Osguthorpe, Biochemistry, 1990, 29, 8223–8228.

18 I. Bahar, B. Erman, T. Haliloglu and R. L. Jernigan, Biochemistry, 1997, 36, 13512–13523.

19 A. Amedei, A. B. M. Linssen and H. J. C. Berendsen, Proteins, 1993, 17, 412–425.

20 A. Polimeno, M. Zerbetto and D. Abergel, J. Chem. Phys., 2019, 150, 184107.

21 A. Polimeno, M. Zerbetto and D. Abergel, J. Chem. Phys., 2019, 150, 184108.

22 H. Goldstein, Classical Mechanics, Addison-Wesley, 1980.

23 R. Zwanzig, Physica, 1964, 30, 1109–1123.

24 R. Zwanzig, J. Stat. Phys., 1973, 9, 215–220.

25 B. Yoon, J. Deutch and J. Freed, J. Chem. Phys., 1975, 62, 4687.

26 R. Pendrill, O. Engström, A. Volpato, M. Zerbetto, A. Polimeno and G. Widmalm, Phys. Chem. Chem. Phys., 2016, 18, 3086–3096.

27 M. Zerbetto, A. Polimeno, D. Kotsyubynskyy, L. Ghalebani, J. Kowalewski, E. Meirovitch, U. Olsson and G. Widmalm, J. Chem. Phys., 2009, 131, 234501.

28 M. Zerbetto, T. Angles d'Ortoli, A. Polimeno and G. Widmalm, J. Phys. Chem. B, 2018, 122, 2287–2294.

29 D. Kotsyubynskyy, M. Zerbetto, M. Soltesova, O. Engström, R. Pendrill, J. Kowalewski, G. Widmalm and A. Polimeno, J. Phys. Chem. B, 2012, 116, 14541–14555.

30 M. Zerbetto, D. Kotsyubynskyy, J. Kowalewski, G. Widmalm and A. Polimeno, J. Phys. Chem. B, 2012, 116, 13159–13171.

14834 | Phys. Chem. Chem. Phys., 2023, 25, 14822–14835

This journal is © the Owner Societies 2023

31 S. Rampino, M. Zerbetto and A. Polimeno, *Molecules*, 2021, **26**, 2418.

32 J. Campeggio, A. Polimeno and M. Zerbetto, *J. Comput. Chem.*, 2019, **40**, 697–705.

33 R. R. Coifman, I. G. Kevrekidis, S. Lafon, M. Maggioni and B. Nadler, *Multiscale Model. Simul.*, 2008, **7**, 842–864.

34 W. Chen, A. R. Tan and A. L. Ferguson, *J. Chem. Phys.*, 2018, **149**, 072312.

This journal is © the Owner Societies 2023

Phys. Chem. Chem. Phys., 2023, **25**, 14822–14835 | **14835**